Saddle Connectors - An Approach to Visualizing the Topological Skeleton of Complex 3D Vector Fields

Holger Theisel *
MPI Informatik Saarbrücken

Tino Weinkauf†
Zuse Institute Berlin

Hans-Christian Hege‡
Zuse Institute Berlin

Hans-Peter Seidel §
MPI Informatik Saarbrücken

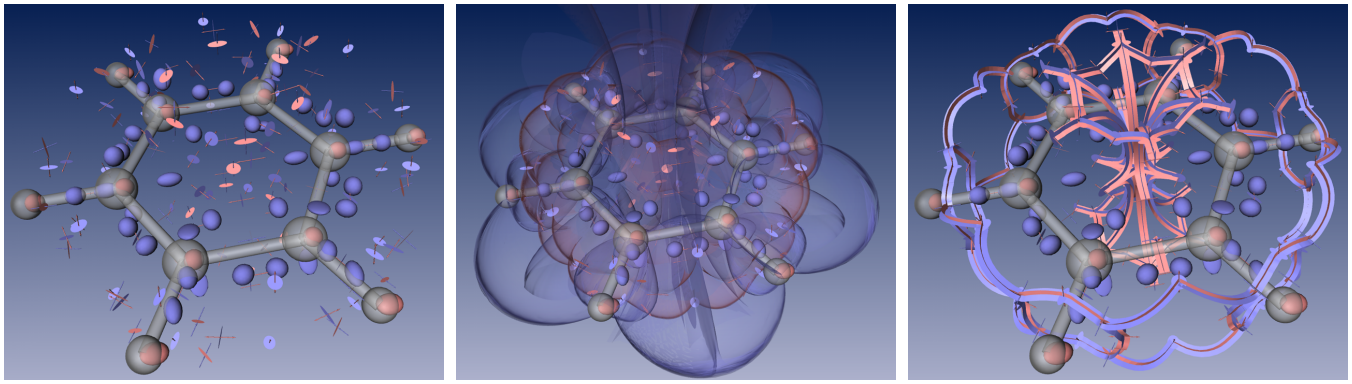

(a) Iconic representation.

(b) Due to the shown separation surfaces, the topological skeleton of the vector field looks visually cluttered.

(c) Visualization of the topological skeleton using saddle connectors.

Figure 1: Topological representations of the benzene data set with 184 critical points.

Abstract

One of the reasons that topological methods have a limited popularity for the visualization of complex 3D flow fields is the fact that such topological structures contain a number of separating stream surfaces. Since these stream surfaces tend to hide each other as well as other topological features, for complex 3D topologies the visualizations become cluttered and hardly interpretable. This paper proposes to use particular stream lines called saddle connectors instead of separating stream surfaces and to depict single surfaces only on user demand. We discuss properties and computational issues of saddle connectors and apply these methods to complex flow data. We show that the use of saddle connectors makes topological skeletons available as a valuable visualization tool even for topologically complex 3D flow data.

Keywords: 3D flow visualization, vector field topology, critical points, separatrices.

*e-mail: theisel@mpi-sb.mpg.de
†e-mail: weinkauf@zib.de
‡e-mail: hege@zib.de
§e-mail: hpseidel@mpi-sb.mpg.de

1 Introduction

Topological methods have become a standard tool in visualizing 2D vector fields. After their introduction as a visualization tool in [Helman and Hesselink 1989], a considerable amount of research has been done to extract, analyze, modify and visualize topological skeletons of 2D vector fields. A topological skeleton basically consists of critical points and certain stream lines called separatrices, which divide the flow domain into areas of different flow behavior. In [Helman and Hesselink 1989], first order critical points are classified by an eigenvalue/eigenvector analysis of the Jacobian matrix, and separatrices starting from saddle points and from attachment and detachment points at no-slip boundaries are considered.

In the following years, these topological concepts have been generalized in several ways. [Scheuermann et al. 1998] treat higher order critical points, i.e. critical points with a possibly vanishing Jacobian. [Trotts et al. 2000] introduce critical points at infinity to find new separatrices. In [de Leeuw and van Liere 1999a], separatrices starting from boundary switch points are discussed. [Wischgoll and Scheuermann 2001] propose a method which detects closed separatrices. Topological methods are used to simplify [de Leeuw and van Liere 1999a; de Leeuw and van Liere 1999b; Tricoche et al. 2000; Tricoche et al. 2001a], smooth [Westermann et al. 2001], compress [Lodha et al. 2000] and design [Theisel 2002] vector fields. Topological skeletons of 2D scalar fields (which can be considered as a special case of 2D vector fields) are treated in [Bajaj and Schikore 1998; Bajaj et al. 1998; Edelsbrunner et al. 2001]. In [Lavin et al. 1998; Batra et al. 1999; Theisel and Weinkauf 2002], topology-based 2D vector field metrics are defined. The topological behavior of time-dependent vector fields is analyzed in [Tricoche et al. 2001b; Tricoche et al. 2002; Theisel and Seidel 2003]. Visualizing the topological skeleton is attractive since even a complex flow behavior can be represented by a limited number of graphical primitives.

Although topological methods are well developed for 2D vector fields, only a few approaches exist for applying them to 3D vector fields. Similar to 2D vector fields, [Helman and Hesselink 1991] proposed methods for detecting and classifying first order critical points by an eigenvalue/eigenvector analysis of the Jacobian matrix. A system for visualizing the topological skeleton of 3D vector fields has been presented in [Globus and Levit 1991]. Topological skeletons of particular analytic 3D vector fields are extracted in [Löffelmann et al. 1998; Hauser and Gröller 2000]. A critical point based metric of 3D vector fields has been presented in [Batra and Hesselink 1999].

All 3D topology methods mentioned above either ignore separatrices, i.e. focus only on a part of the topology, or they were applied only to vector fields with a rather simple topology, i.e. with a small number of critical points and separatrices. One reason for this seems to be that separatrices of 3D vector fields consist also of stream surfaces – a fact which creates a number of problems. In particular, we see the following reasons why topological visualization of 3D vector fields is still less common than of 2D vector fields:

- The integration of stream surfaces is computationally more involved and less stable than the integration of stream lines, since convergence and divergence effects on the stream surface may occur.

- The visualization of the topological skeleton of a vector field requires simultaneous visualization of a higher number of stream surfaces, which very soon leads to visually cluttered representations. Figure 1a and 1b depict an example. In Figure 1a, only the critical points of a 3D vector field are visualized using icons. An additional visualization of the separation surfaces as in Figure 1b creates visual clutter, since the surfaces hide each other as well as the critical points. This problem remains, even if the separation surfaces are rendered in a semi-transparent mode.

A number of solutions have been proposed for the first problem, see [Hultquist 1992; Gelder 2001; Scheuermann et al. 2001; van Wijk 1993].

In this paper, we tackle the second problem. In order to create sparse visual representations that avoid occlusion and minimize visual clutter, we propose to represent the separation surfaces as a finite number of stream lines. These stream lines are the intersection curves of the separation surfaces. We call them *saddle connectors* because they start and end in saddle points of the vector field.

The saddle connectors indicate only the approximate run of the separation surfaces and of course cannot completely substitute them. A possible procedure is to always depict the saddle connectors and interactively, on user demand, additionally display *single* separating surfaces.

The rest of the paper is organized as follows: Section 2 restates the basic concepts of 3D vector field topology. Section 3 introduces the concept of saddle connectors and discusses their computation and visual representation. Section 4 shows the results of applying saddle connectors to 3D vector fields of a complex topology. Section 5 draws conclusions and mentions future work.

2 The Topology of a 3D Vector Field

Topological structures of 3D vector fields are well-understood in the visualization community for many years [Helman and Hesselink 1991; Asimov 1993; Chong et al. 1990; Philippou and Strickland 1997]. In this section, we collect the most important concepts and properties.

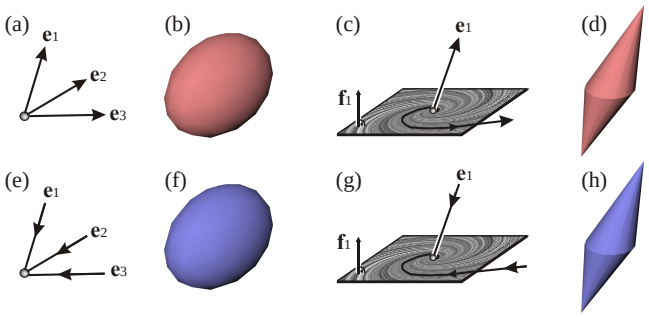

Figure 2: Sources and sinks; (a) repelling node and (b) its icon; (c) repelling focus and (d) its icon; (e) attracting node and (f) its icon; (g) attracting focus and (h) its icon.

2.1 Critical points

Given a 3D vector field $\mathbf{v} : \mathbb{E}^3 \rightarrow \mathbb{R}^3$, a first order critical point $\mathbf{x}_0$ (i.e., a point $\mathbf{x}_0$ with $\mathbf{v}(\mathbf{x}_0) = \mathbf{0}$ and $\det(\mathbf{J}_\mathbf{v}(\mathbf{x}_0)) \neq 0$, where $\mathbf{J}_\mathbf{v}(\mathbf{x}) = \nabla\mathbf{v}(\mathbf{x})$ is the Jacobian matrix of $\mathbf{v}$) can be classified by an eigenvalue/eigenvector analysis of $\mathbf{J}_\mathbf{v}(\mathbf{x}_0)$. Let $\lambda_1, \lambda_2, \lambda_3$ be the eigenvalues of $\mathbf{J}_\mathbf{v}(\mathbf{x}_0)$ ordered according to their real parts, i.e. $Re(\lambda_1) \leq Re(\lambda_2) \leq Re(\lambda_3)$. Furthermore, let $\mathbf{e}_1, \mathbf{e}_2, \mathbf{e}_3$ be the corresponding eigenvectors, and let $\mathbf{f}_1, \mathbf{f}_2, \mathbf{f}_3$ be the eigenvectors of the transposed Jacobian $(\mathbf{J}_\mathbf{v}(\mathbf{x}_0))^T$ corresponding to $\lambda_1, \lambda_2, \lambda_3$. (Note that $\mathbf{J}$ and $\mathbf{J}^T$ have the same eigenvalues but not necessarily the same eigenvectors.) Concerning the real parts of the eigenvalues, the following classification of critical points is possible:

- sources: $0 < Re(\lambda_1) \leq Re(\lambda_2) \leq Re(\lambda_3)$
- repelling saddles: $Re(\lambda_1) < 0 < Re(\lambda_2) \leq Re(\lambda_3)$
- attracting saddles: $Re(\lambda_1) \leq Re(\lambda_2) < 0 < Re(\lambda_3)$
- sinks: $Re(\lambda_1) \leq Re(\lambda_2) \leq Re(\lambda_3) < 0$

Each of these classes can be further divided into two stable[1] subclasses by deciding if imaginary parts in the eigenvalues are present. Since vector fields usually consist of a finite number of critical points, an iconic representation is the appropriate visualization approach. Several icons have been proposed in the literature, see [Helman and Hesselink 1991; Globus and Levit 1991; Löffelmann et al. 1998; Hauser and Gröller 2000]. In the following we describe the different classes of critical points as well as the icons we used for their visual representation. We colored these icons depending on the flow behavior: Attracting parts (inflow) are colored blue, while repelling parts (outflow) are colored red.

Sources and Sinks

A source $\mathbf{x}_{So}$ is characterized by the fact that in its neighborhood all stream lines diverge from $\mathbf{x}_{So}$. The two stable subclasses are repelling nodes and repelling foci.

A *repelling node* is characterized by the absence of imaginary parts in $\lambda_1, \lambda_2, \lambda_3$, and $\mathbf{e}_1, \mathbf{e}_2, \mathbf{e}_3$ are linearly independent (Figure 2a). To visualize a repelling node, we use a red ellipsoid with a shape determined by the eigenvectors and eigenvalues of the Jacobian (Figure 2b).

A *repelling focus* is characterized by the presence of two eigenvalues with imaginary parts, say λ_2, λ_3. In this case, the only real eigenvector $\mathbf{e}_1$ of $\mathbf{J}$ describes the direction of straight outflow. In

[1] A critical point in $\mathbf{v}$ is called stable if a small perturbation of $\mathbf{v}$ does not change the classification of the critical point.

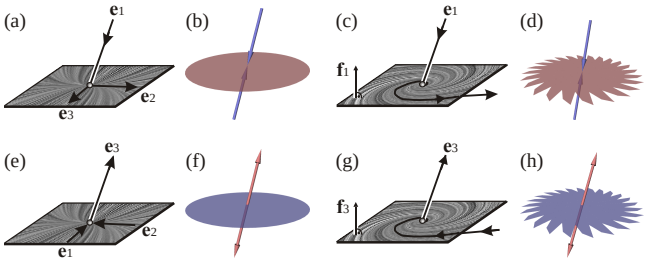

Figure 3: Repelling and attracting saddles; (a) repelling node saddle and (b) its icon; (c) repelling focus saddle and (d) its icon; (e) attracting node saddle and (f) its icon; (g) attracting focus saddle and (h) its icon.

addition, there is a plane in which a 2D repelling focus behavior appears. This plane is perpendicular to the only real eigenvector $\mathbf{f}_1$ of $\mathbf{J}^T$ (Figure 2c). As an icon, we used a red double cone representing the outflow plane and the outflow direction by its shape (Figure 2d).

A sink $\mathbf{x}_{Si}$ can be considered as an inverse source: in its neighborhood all stream lines collapse into $\mathbf{x}_{Si}$. The two subcases are *attracting nodes* (Figures 2e-f) and *attracting foci* (Figures 2g-h).

Repelling Saddles and Attracting Saddles

A repelling saddle $\mathbf{x}_R$ has one direction of inflow behavior (called *inflow direction*) and a plane in which a 2D outflow behavior occurs (called *outflow plane* through $\mathbf{x}_R$). For all other directions around $\mathbf{x}_R$, the stream lines do not touch $\mathbf{x}_R$. The two stable subclasses are repelling node saddles and repelling focus saddles.

A *repelling node saddle* has no imaginary parts in $\lambda_1, \lambda_2, \lambda_3$, and $\mathbf{e}_1, \mathbf{e}_2, \mathbf{e}_3$ are linearly independent (Figure 3a). Its icon includes a red ellipse denoting the outflow plane defined by $\mathbf{e}_2, \mathbf{e}_3$ and λ_2, λ_3, while a blue arrow pointing to the center of the ellipse represents the inflow direction (Figure 3b).

A *repelling focus saddle* is characterized by $Im(\lambda_2) = -Im(\lambda_3) \neq 0$. Here, the only real eigenvector $\mathbf{e}_1$ of $\mathbf{J}$ describes the inflow direction. The only real eigenvector $\mathbf{f}_1$ of $\mathbf{J}^T$ describes the plane with the 2D repelling focus behavior (Figures 3c-d).

An attracting saddle $\mathbf{x}_A$ can be interpreted as an inverse version of a repelling saddle. It has one direction of outflow behavior (*outflow direction*) and a plane in which a 2D inflow behavior appears (*inflow plane* through $\mathbf{x}_A$). The two stable subclasses are *attracting node saddles* without imaginary parts of the eigenvalues (Figures 3e-f) and *attracting focus saddles* (Figures 3g-h).

In addition to the kinds of critical points described above, a number of unstable versions of sources, sinks and repelling/attracting saddles exist. Also, two further classes of unstable critical points exist which do not belong to any of the above-mentioned classes: attracting centers and repelling centers. A repelling center is characterized by $Re(\lambda_1) = Re(\lambda_2) = 0 < Re(\lambda_3)$ and $Im(\lambda_1) = -Im(\lambda_2) \neq 0$. It consists of one direction $\mathbf{e}_3$ of outflow behavior and one plane perpendicular to $\mathbf{f}_3$ with a 2D circulating behavior. An attracting center has $Re(\lambda_1) < 0 = Re(\lambda_2) = Re(\lambda_3)$ and $Im(\lambda_2) = -Im(\lambda_3) \neq 0$. The inflow direction is defined by $\mathbf{e}_1$ and the 2D circulating behavior can be found in the plane perpendicular to $\mathbf{f}_1$.

Higher order critical points are not considered in this paper.

2.2 Separatrices

Separatrices are curves or surfaces which separate regions of different flow behavior. Since around sources and sinks a homogeneous flow behavior is present (either a complete outflow or inflow), sources and sinks do not contribute to separatrices. A repelling saddle $\mathbf{x}_R$ creates two separatrices: one separation curve (which is a stream line starting in $\mathbf{x}_R$ in the inflow direction by backward integration) and a separation surface (which is a stream surface starting in the outflow plane by forward integration). Figure 4 gives an illustration. A similar statement holds for attracting saddles.

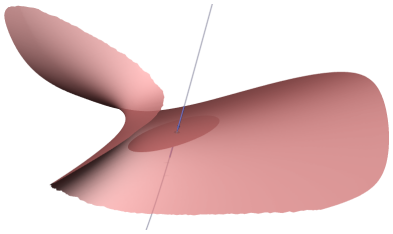

Figure 4: Separatrices originating from a repelling node saddle.

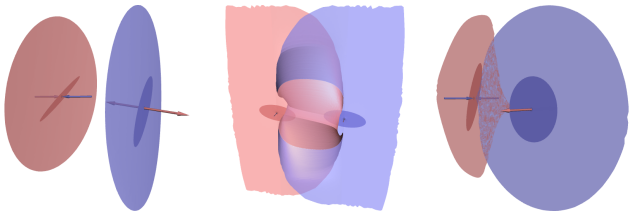

(a) No intersection. (b) Two intersection curves. (c) The separation surfaces collapse.

Figure 5: Intersection of separation surfaces.

Further kinds of separatrices are possible, for instance separation surfaces emanating from boundary switch curves, or closed stream lines. However, in this paper we restrict ourselves to separatrices starting from saddle points.

As already shown in Figure 1b, the complete visualization of a rather complex topological skeleton does not give visually pleasing results. Because of this, we propose an alternative approach as described in the next section.

3 Saddle Connectors

This section introduces the new concept of saddle connectors and discusses properties and computational attempts. The basic idea of saddle connectors is to consider the intersection of the separation surfaces of two saddle points. For this intersection, the following cases are possible:

- The separation surfaces of two saddles have no intersection (Figure 5a).
- The separation surfaces have one intersection curve (Figure 6a).
- The separation surfaces have more than one, but a finite number of intersection curves (Figure 5b).
- The separation surfaces partially collapse. In this case, the intersection of the separation surfaces is a surface (Figure 5c).

We define saddle connectors as follows (Figure 6 gives an illustration):

Definition 1 *Let $\mathbf{v}$ be a 3D vector field, and let $\mathbf{x}_1$ and $\mathbf{x}_2$ be two saddle points in $\mathbf{v}$. We consider the intersection of the two separation surfaces starting in the outflow/inflow planes of $\mathbf{x}_1$ and $\mathbf{x}_2$. If this intersection is a curve, we call it a saddle connector.*

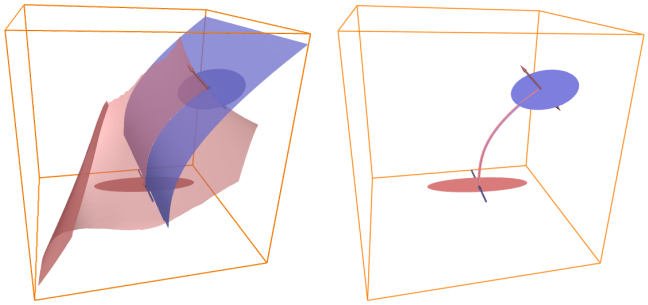

(a) Separation surfaces of the saddles.

(b) The intersection of the separation surfaces is the saddle connector.

Figure 6: Definition of saddle connectors.

Note that this definition excludes cases of partially collapsing separation surfaces. This is justified by the fact that this case can be seen as an unstable situation in the vector field.

3.1 Properties of Saddle Connectors

An intersection of the separating surfaces of two saddle points can only exist if one of the saddles is an attracting saddle and the other one is a repelling saddle. To see this, imagine for instance two attracting saddles[2] $\mathbf{x}_{A1}$, $\mathbf{x}_{A2}$, and suppose that a certain point $\mathbf{p}$ lies on both separation surfaces of $\mathbf{x}_{A1}$ and $\mathbf{x}_{A2}$. Then the stream line starting from $\mathbf{p}$ in forward direction must both pass through $\mathbf{x}_{A1}$ and $\mathbf{x}_{A2}$, which contradicts to basic properties of critical points and stream lines.

Also from definition 1 we obtain that a saddle connector is a stream line which starts in the outflow plane of a repelling saddle $\mathbf{x}_R$ and ends in the inflow plane of an attracting saddle $\mathbf{x}_A$. This holds because for every stream surface, the stream line starting from any point on this surface lies completely in the stream surface. Thus, if a point $\mathbf{p}$ lies on both separation surfaces of $\mathbf{x}_R$ and $\mathbf{x}_A$, the whole stream line starting in $\mathbf{p}$ in forward and backward direction lies in both separation surfaces. Therefore, this stream line connects both saddles.

One way of analyzing separation surfaces is asking for their boundary curves. If a separation surface does not have a strong diverging behavior, its boundary curve gives a good deal of information about its behavior in the 3D domain of $\mathbf{v}$. The boundary curve of a separation surface may be a closed curve on the boundary of the domain of $\mathbf{v}$. It is also possible that the separation surface ends in a number of sinks *or* sources. In this case, there is a relation between the saddle connectors and the boundary curves of the separation surfaces. To compute the boundary curve of the separation surface of a repelling saddle $\mathbf{x}_R$, we can compute the saddle connectors of $\mathbf{x}_R$ with all attracting saddles. Then we consider the repelling separation curves of all attracting saddles which share a saddle connector with $\mathbf{x}_R$. If the union of all these curves forms a closed curve, this closed curve describes the boundary curve of the separation surface of $\mathbf{x}_R$. Figure 7 shows an example.

3.2 Seeding and Integrating the Separation Surfaces

Since saddle connectors are intersections of separation surfaces their integration process will play a substantial role in the computation of the connectors.

[2]Or two repelling saddles.

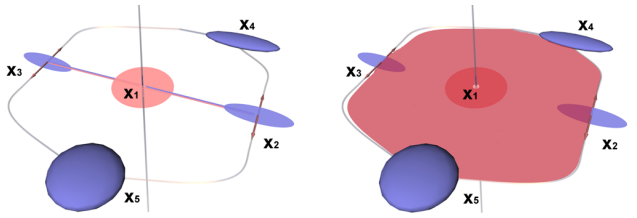

Figure 7: (left) The repelling saddle $\mathbf{x}_1$ has saddle connectors to the attracting saddles $\mathbf{x}_2$ and $\mathbf{x}_3$. The repelling separation curves of $\mathbf{x}_2$ and $\mathbf{x}_3$ end in the sinks $\mathbf{x}_4$ and $\mathbf{x}_5$, and form a closed curve. (right) The separation curves of $\mathbf{x}_2$ and $\mathbf{x}_3$ are the boundary curves of the separation surface of $\mathbf{x}_1$.

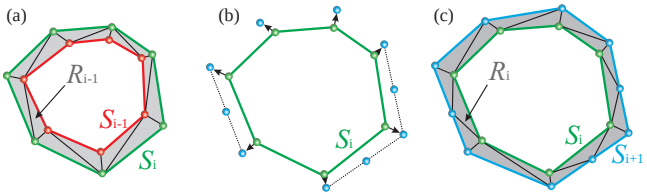

Figure 8: Computing time ribbons of a separation surface; (a) the time line S_{i-1} consists of the red points and edges, the time line S_i is colored green; the time ribbon R_{i-1} is described by the triangulation between S_{i-1} and S_i (gray area); (b) to compute the time ribbon R_i, we apply one numerical integration step to each point of S_i and adaptively insert/remove points; this way we obtain S_{i+1} (blue points); (c) the new time ribbon R_i is the triangulation between S_i and S_{i+1} (gray area).

To integrate the separation surface of a saddle point $\mathbf{x}_0$, we place n_0 points in an equidistant manner on a small circle in the outflow/inflow plane around $\mathbf{x}_0$. They serve as the seeding points of the separation surface. This closed polygon $S_0 = (\mathbf{s}_{0,0}, ..., \mathbf{s}_{n_0,0})$ can be considered as the time line of the separation surface for the time t_0.

This kind of seeding yields good results for most topologies except for focus saddles with strong circulation, where the stream lines would intersect the seeding circle. In this case we place the seeding points on a small line in the outflow/inflow plane starting at the critical point.

The integration of the separation surfaces is done using a technique similar to the one proposed by [Hultquist 1992] or [Stalling 1998]. To get the time line S_{i+1}, we apply one step of a numerical stream line integration[3] to all points of $S_i = (\mathbf{s}_{0,i}, ..., \mathbf{s}_{n_i,i})$. To the n_i new points obtained this way, an adaptive thinning or enrichment is applied similar to [Stalling 1998]. This results in a new number of points for $S_{i+1} = (\mathbf{s}_{0,i+1}, ..., \mathbf{s}_{n_{i+1},i+1})$. By applying a triangulation between S_i and S_{i+1}, we obtain a *time ribbon* R_i. Figure 8 gives an illustration.

For each stream line a parameter α is stored, which determines its starting point on the seeding rake[4]. Consider two neighboring points $\mathbf{s}_{k,i}$ and $\mathbf{s}_{k+1,i}$ with their corresponding parameters α_k and α_{k+1}. For every $\alpha' \in (\alpha_k, \alpha_{k+1})$, the integration of the stream line from the seeding rake gives – after i time steps – a new point between $\mathbf{s}_{k,i}$ and $\mathbf{s}_{k+1,i}$. This way of constructing a new point on the time line S_i is used both for the adaptive enrichment described above and for the refinement step in the algorithm described below.

[3]We used a fourth-order Runge-Kutta integration. The direction of the integration depends on the topology of the originating saddle: Forward integration is used for $\mathbf{x}_R$ and backward integration for $\mathbf{x}_A$.

[4]Seeding circle or seeding line.

3.3 Computing the Saddle Connector Between two Saddles

Several approaches for finding saddle connectors can be thought of. We want to discuss two of them here.

The first approach follows directly the definition of saddle connectors by integrating the separation surfaces and intersecting their triangle mesh representations.

To ensure that the resulting intersection curves start and end near the saddles, each surface needs to be integrated until it comes very close to all other saddles that share a connector with the originating saddle. Only in this case, the resulting intersection curves start and end near the critical points. Our experience has shown that especially for topologies with circulating flow behavior like focus saddles, this is hard to ensure. Furthermore, this approach does not only need a lot of integration steps but also a considerable amount of memory as one needs to hold all generated triangles.

We propose another algorithm with less memory consumption, which enables us to find saddle connectors with less integration steps than the first approach. We utilize the fact that saddle connectors are particular stream lines: knowing one (non–critical) point of a stream line is enough to integrate the whole line. Unfortunately, the only prior known points of a saddle connector are its connected saddles. Both are critical points and do not suffice to uniquely determine the stream line.

Consider a repelling saddle $\mathbf{x}_R$ and an attracting saddle $\mathbf{x}_A$. As their separating surfaces start at the seeding rakes, the starting and ending points of the saddle connector lie on the rakes as well. We apply a simultaneous integration of the stream surfaces until an intersection point $\mathbf{p}$ is found. This point lies close to the saddle connector, but due to the triangle approximation of the surfaces it is not necessarily on the connector itself. Let $\mathbf{p}'$ be the point on the connector which is closest to $\mathbf{p}$. $\mathbf{p}'$ has two corresponding seeding points – one on each rake. They can be described by the parameters $\alpha' \in (\alpha_k, \alpha_{k+1})$ and $\beta' \in (\beta_h, \beta_{h+1})$ and are found by applying a refinement.

To find $\mathbf{p}$ we only need to simultaneously compute the time ribbons R_i^R of $\mathbf{x}_R$ and R_i^A of $\mathbf{x}_A$, and check them for intersection. For this it is sufficient to check if the last time line of $\mathbf{x}_R$ intersects the last time ribbon of $\mathbf{x}_A$ and vice versa. This means that we do not have to check the triangular strips themselves for intersection, but line segments with triangular strips. Figure 9 illustrates the process of finding a saddle connector and algorithm 1 gives a detailed description.

For two reasons this algorithm may find more than one intersection point. First, the considered saddles may have multiple connectors (see Figure 5b). Second, we perform two intersection tests after each surface propagation, and in many cases[5] both produce results at the same time step. The two points resulting from this are very close to each other, and one of them can be deleted safely. The algorithm terminates after finding a certain maximal number of intersection points (or if a maximal time is reached).

Algorithm 1 depends on a number of parameters: the step size of the stream line integration, the number of initial seed points, and the thresholds for inserting or deleting points for a new time line. For all these values, a reasonable compromise has to be found between performance and accuracy.

An advantage of algorithm 1 is that it avoids stream line integration in numerically complicated regions (i.e., in regions in which the separation surface of a saddle comes close to another saddle and therefore has a strongly diverging behavior). Also, the algorithm stops after a certain pre-defined number n_{max} of maximal connectors is found[6]. This leads to a significant reduction of necessary integration steps. Finally, note that memory is hardly a problem, since from each separation surface only a time ribbon (represented by a triangular strip) is stored at any stage of the algorithm.

[5] But not in all cases: If we use different step sizes for the integration of the surfaces, these two tests may result in only one intersection point. Thats why two tests are performed. Otherwise one time ribbon could "jump" over the other.

[6] In our implementation we set $n_{max} = 1$ and therefore stopped the algorithm after finding one connector between two saddles.

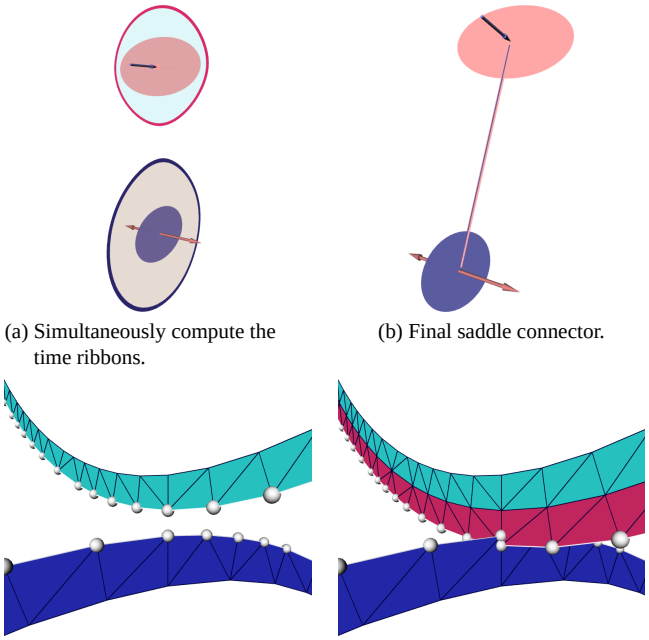

(a) Simultaneously compute the time ribbons.

(b) Final saddle connector.

(c) Closeup shortly before an intersection is found.

(d) Intersection is found.

Figure 9: Computing a saddle connector.

Algorithm 1 Finding intersections between separation surfaces

$\mathbf{p}[\,] = \texttt{EmptyArrayOfPoints}()$
$S_0^A = \texttt{Seed}(\mathbf{x}_A)$
$S_0^R = \texttt{Seed}(\mathbf{x}_R)$

$S_1^A = \texttt{PropagateSurface}\,(\mathbf{x}_A, S_0^A, t_1)$
$R_0^A = \texttt{Triangulate}\,(S_1^A, S_0^A)$

$i = 0$
while $(\texttt{Size}\,(\mathbf{p}[\,]) < n_{max}) \wedge (t_i < t_{max})$ **do**
  $S_{i+1}^R = \texttt{PropagateSurface}\,(\mathbf{x}_R, S_i^R, t_{i+1})$
  $R_i^R = \texttt{Triangulate}\,(S_{i+1}^R, S_i^R)$

  $\mathbf{p}[\,] += \texttt{GetIntersectionPoints}\,(S_{i+1}^R, R_i^A)$
  $\mathbf{p}[\,] += \texttt{GetIntersectionPoints}\,(S_{i+1}^A, R_i^R)$

  $S_{i+2}^A = \texttt{PropagateSurface}\,(\mathbf{x}_A, S_{i+1}^A, t_{i+2})$
  $R_{i+1}^A = \texttt{Triangulate}\,(S_{i+2}^A, S_{i+1}^A)$

  $\mathbf{p}[\,] += \texttt{GetIntersectionPoints}\,(S_{i+1}^R, R_{i+1}^A)$
  $\mathbf{p}[\,] += \texttt{GetIntersectionPoints}\,(S_{i+2}^A, R_i^R)$

  $\texttt{FreeMemory}\,(S_i^R, R_i^R, S_{i+1}^A, R_i^A)$
  $i = i + 1$
end while

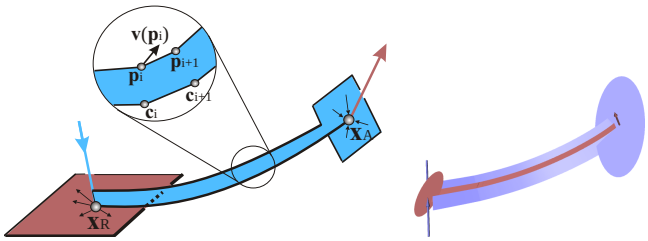

(a) Computing the flow ribbon of the connector between $\mathbf{x}_R$ and $\mathbf{x}_A$ belonging to the separation surface of $\mathbf{x}_A$.

(b) Double flow ribbon used for representing a saddle connector.

Figure 10: Visual representation of saddle connectors.

3.4 Computing all Saddle Connectors

To catch the topology of the whole 3D vector field, we have to compute the saddle connectors between all saddle points. A naive approach to do so – applying the algorithm of section 3.3 to any pair of repelling and attracting saddles – is not an appropriate solution because the time-consuming integration of a separation surface is repeated again and again.

Instead, we avoid a multiple computation of a separation surface by grouping all attracting and all repelling saddles and applying a slightly modified version of algorithm 1 on these two groups: after computing a new time ribbon for all saddles in one group, they have to be checked against all current time ribbons of the other group.

If a time ribbon of a saddle leaves the domain of the vector field or collapses to a number of single points, the time ribbon is excluded from further consideration. This algorithm has a time complexity of $O(n^2)$ where n is the number of saddle points in the vector field.

3.5 Visual Representation of Saddle Connectors

Once saddle connectors are computed, we have to find a graphical representation. The simplest way is to use a line representation similar to stream lines. However, since saddle connectors are defined as the intersection of two separation surfaces, we can also visualize the orientation of the separation surfaces in the neighborhood of the saddle connector. To do so, we use a double flow ribbon approach as shown in Figure 10b.

Given are the repelling saddle $\mathbf{x}_R$, the attracting saddle $\mathbf{x}_A$ and their saddle connector represented by a sequence $\mathbf{c}_0, ..., \mathbf{c}_m$ of points. To construct the flow ribbon belonging to the separation surface of $\mathbf{x}_A$, we have to find a sequence $\mathbf{p}_0, ..., \mathbf{p}_m$ of points in such a way that the distance between $\mathbf{c}_i$ and $\mathbf{p}_i$ is constant, and the line segments $(\mathbf{c}_i, \mathbf{p}_i)$ are in the separation surface of $\mathbf{x}_A$ for all i. To do so, we set $\mathbf{p}_0 = \mathbf{x}_R + \lambda \cdot \mathbf{e}$ where $\mathbf{e}$ is the only eigenvector of $\mathbf{J}_\mathbf{v}(\mathbf{x}_R)$ which has a negative eigenvalue, and λ is chosen in such a way that $\mathbf{c}_0$ and $\mathbf{p}_0$ have a pre-defined constant distance. Then the point $\mathbf{p}_{i+1}$ is constructed from $\mathbf{c}_i$, $\mathbf{c}_{i+1}$ and $\mathbf{p}_i$ by the following conditions:

- $(\mathbf{p}_{i+1} - \mathbf{c}_{i+1}) \perp (\mathbf{c}_{i+1} - \mathbf{c}_i)$
- $\det(\mathbf{p}_i - \mathbf{c}_i\ ,\ \mathbf{v}(\mathbf{p}_i)\ ,\ \mathbf{p}_{i+1} - \mathbf{c}_{i+1}) = 0$, i.e., $(\mathbf{p}_{i+1} - \mathbf{c}_{i+1})$ lies in the plane given by the 3 points $\mathbf{c}_i, \mathbf{p}_i, \mathbf{p}_i + \mathbf{v}(\mathbf{p}_i)$.
- $\|\mathbf{p}_{i+1} - \mathbf{c}_{i+1}\| = \|\mathbf{p}_i - \mathbf{c}_i\|$

Figure 10a gives an illustration. In a similar way we compute the flow ribbon which belongs to the separation surface of $\mathbf{x}_R$.

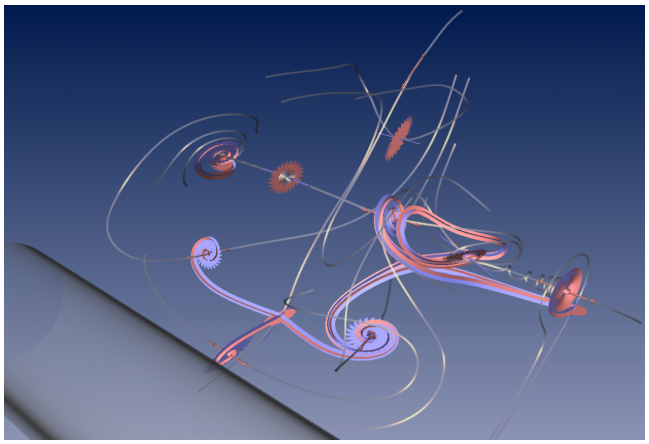

Figure 11: Flow behind a circular cylinder. Topological skeleton using saddle connectors.

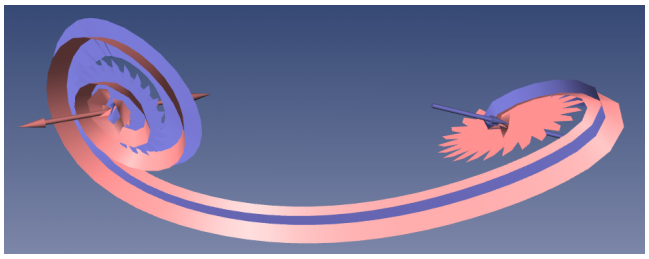

Figure 12: Flow behind a circular cylinder. Close-up of a saddle connector between two focus saddles.

4 Applications

We applied the concept of saddle connectors to two 3D data sets of a rather complex topology.

Figures 11 – 12 visualize a snapshot of a transitional wake behind a circular cylinder [Zhang et al. 1995]. This flow exhibits periodic vortex shedding leading to the well known von Kármán vortex street. This phenomenon plays an important role in many industrial applications, like mixing in heat exchangers or mass flow measurements with vortex counters. However, this vortex shedding can lead to undesirable periodic forces on obstacles, like chimneys, buildings, bridges and submarine towers.

This data set was derived from a direct numerical simulation of the Navier-Stokes equation by Gerd Mutschke [Mutschke 2003]. The data resolves the so-called 'mode A' of the 3D transition at a Reynolds number of 200 and at a spanwise wavelength of 4 diameters. The figures display a small near-wake region of a large computational domain. All 13 fixed points are contained in the shown domain and span the topological skeleton of the incompressible velocity field.

The topology enables to reduce a high-dimensional data set to a simple conceptual flow representation from which qualitative conclusions can be drawn. The skeleton elucidates the symmetry of the mode A with respect to a plane which is perpendicular to the cylinder axis. The spanwise and transverse connectedness of the distributed saddle points of a single snapshot already indicates the experimentally observed good mixing properties of vortex shedding. The saddle points, for instance, are regions of enhanced stretching. Our algorithm detects and visualizes 9 saddle connectors in the data set.

Figures 1 and 14 visualize the electrostatic field around a ben-

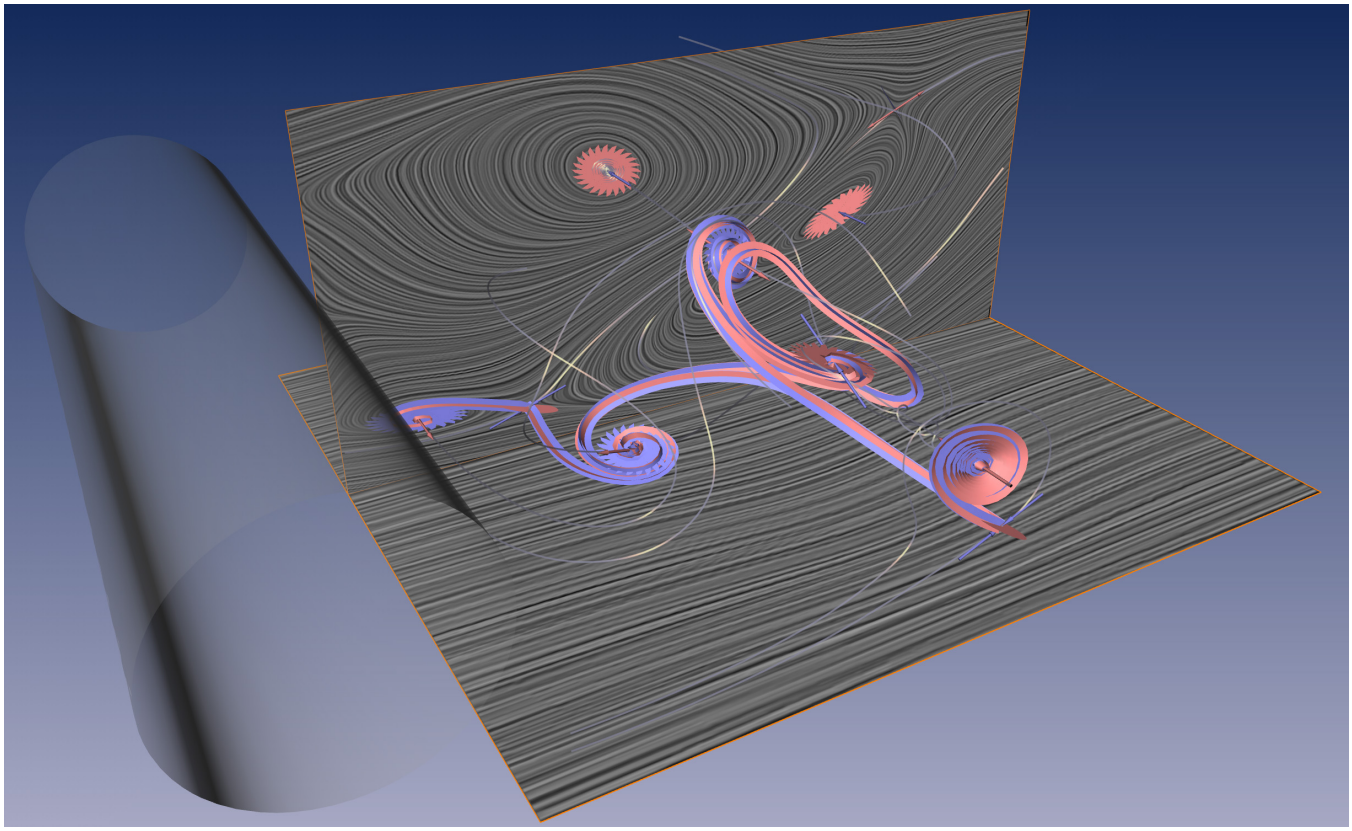

Figure 13: Flow behind a circular cylinder. 13 critical points and 9 saddle connectors have been detected and visualized. Additional LIC planes have been placed to show the correspondence between the skeleton and the flow.

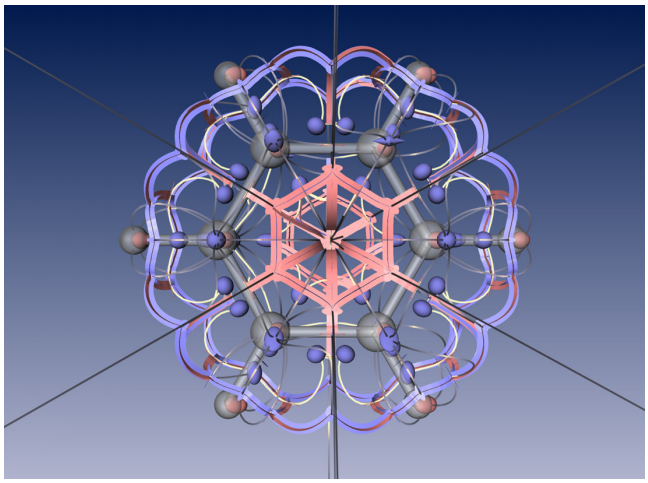

Figure 14: Benzene data set: critical points, separation curves and saddle connectors.

zene molecule. This data set was calculated on a 101^3 regular grid using the fractional charges method described in [Stalling and Steinke 1996]. It consists of 184 first order critical points. The saddle connector visualizations show 129 connectors between 78 attracting and 43 repelling saddles. This example shows that saddle connectors give expressive visualizations even for topologically complex 3D vector fields.

5 Conclusions

We have introduced the concept of saddle connectors as a new approach to visualizing the topological skeleton of complex 3D vector fields. Although the theory of topological skeletons of 3D vector fields is well understood in the visualization community, expressive visualizations have only been obtained for topologically simple data sets (or by a restriction to only a part of the topology). Saddle connectors yield for the first time expressive visualizations of complex topological skeletons with a higher number of critical points and separatrices.

Saddle connectors can be interpreted as a "skeleton of a skeleton" concept. In fact, a geometrically simplified representation is computed for the system of separation surfaces. Although we have shown that this is a useful compromise between the amount of coded information and the expressiveness of the visualization for complex topological skeletons, one important property of the topological skeleton is lost: the unique partition of the vector field into areas of similar flow behavior. In fact, using saddle connectors it is no longer possible to uniquely infer the flow behavior of $\mathbf{v}$ from any point of the domain. Nevertheless, due to the usage of a double flow ribbon representation of the saddle connectors, the user can comprehend the topology of the 3D vector field as well as the flow behavior in particular points of the domain. Furthermore, with the possibility to interactively demand the display of *single* separation surfaces, the user can explore the partitioning of the whole domain.

In future work we will reduce the number of parameters for steering the computation of saddle connectors in our current implementation. Furthermore, we plan to combine the concept of saddle connectors with alternative stream surface integration methods

(e.g. [Scheuermann et al. 2001]), if a higher accuracy is necessary in certain regions of the vector field.

6 Acknowledgements

We thank Bernd R. Noack for the fruitful discussions and supply of simulation data which was kindly provided by Gerd Mutschke.

All visualizations in this paper have been created using AMIRA – a system for advanced 3D visualization and volume modeling [Stalling et al. to appear] (see `http://amira.zib.de/`).

References

ASIMOV, D. 1993. Notes on the topology of vector fields and flows. Tech. rep., NASA Ames Research Center. RNR-93-003.

BAJAJ, C., AND SCHIKORE, D. 1998. Topology-preserving data simplification with error bounds. *Comput. & Graphics 22*, 1, 3–12.

BAJAJ, C., PASCUCCI, V., AND SCHIKORE, D. 1998. Visualization of scalar topology for structural enhancement. In *Proc. IEEE Visualization '98*, 51–58.

BATRA, R., AND HESSELINK, L. 1999. Feature comparisons of 3-D vector fields using earth mover's distance. In *Proc. IEEE Visualization '99*, 105–114.

BATRA, R., KLING, K., AND HESSELINK, L. 1999. Topology based vector field comparison using graph methods. In *Proc. IEEE Visualization '99, Late Breaking Hot Topics*, 25–28.

CHONG, M. S., PERRY, A. E., AND CANTWELL, B. J. 1990. A general classification of three-dimensional flow fields. *Physics of Fluids A 2*, 5, 765–777.

DE LEEUW, W., AND VAN LIERE, R. 1999. Collapsing flow topology using area metrics. In *Proc. IEEE Visualization '99*, D. Ebert, M. Gross, and B. Hamann, Eds., 149–354.

DE LEEUW, W., AND VAN LIERE, R. 1999. Visualization of global flow structures using multiple levels of topology. In *Data Visualization 1999. Proc. VisSym 99*, 45–52.

EDELSBRUNNER, H., HARER, J., AND ZOMORODIAN, A. 2001. Hierarchical morse complexes for piecewise linear 2-manifolds. In *Proc. 17th Sympos. Comput. Geom. 2001*.

GELDER, A. V. 2001. Stream surface generation for fluid flow solutions on curvilinear grids. In *Data Visualization 2001. Proc. VisSym 01*.

GLOBUS, A., AND LEVIT, C. 1991. A tool for visualizing of three-dimensional vector fields. In *Proc. IEEE Visualization '91*, IEEE Computer Society Press, 33–40.

HAUSER, H., AND GRÖLLER, E. 2000. Thorough insights by enhanced visualization of flow topology. In *9th international symposium on flow visualization*.

HELMAN, J., AND HESSELINK, L. 1989. Representation and display of vector field topology in fluid flow data sets. *IEEE Computer 22*, 8 (August), 27–36.

HELMAN, J., AND HESSELINK, L. 1991. Visualizing vector field topology in fluid flows. *IEEE Computer Graphics and Applications 11* (May), 36–46.

HULTQUIST, J. 1992. Constructing stream surfaces in steady 3D vector fields. In *Proc. IEEE Visualization '92*, 171–177.

LAVIN, Y., BATRA, R., AND HESSELINK, L. 1998. Feature comparisons of vector fields using earth mover's distance. In *Proc. IEEE Visualization '98*, 103–109.

LODHA, S., RENTERIA, J., AND ROSKIN, K. 2000. Topology preserving compression of 2D vector fields. In *Proc. IEEE Visualization 2000*, 343–350.

LÖFFELMANN, H., DOLEISCH, H., AND GRÖLLER, E. 1998. Visualizing dynamical systems near critical points. In *Spring Conference on Computer Graphics and its Applications*, 175–184.

MUTSCHKE, G., 2003. private communication.

PHILIPPOU, P. A., AND STRICKLAND, R. N. 1997. Vector field analysis and synthesis using three dimensional phase portraits. *Graphical Models and Image Processing 59* (November), 446–462.

SCHEUERMANN, G., KRÜGER, H., MENZEL, M., AND ROCKWOOD, A. 1998. Visualizing non-linear vector field topology. *IEEE Transactions on Visualization and Computer Graphics 4*, 2, 109–116.

SCHEUERMANN, G., BOBACH, T., MAHROUS, H. H. K., HAMANN, B., JOY, K., AND KOLLMANN, W. 2001. A tetrahedra-based stream surface algorithm. In *Proc. Visualization 01*, 151 – 158.

STALLING, D., AND STEINKE, T. 1996. Visualization of vector fields in quantum chemistry. Tech. rep., ZIB Preprint SC-96-01. ftp://ftp.zib.de/pub/zib-publications/reports/SC-96-01.ps.

STALLING, D., WESTERHOFF, M., AND HEGE, H.-C. to appear. Amira – an object oriented system for visual data analysis. In *Visualization Handbook*, Academic Press, C. R. Johnson and C. D. Hansen, Eds.

STALLING, D. 1998. *Fast Texture-based Algorithms for Vector Field Visualization*. PhD thesis, FU Berlin, Department of Mathematics and Computer Science.

THEISEL, H., AND SEIDEL, H.-P. 2003. Feature flow fields. In *Data Visualization 2003. Proc. VisSym 03*, 141–148.

THEISEL, H., AND WEINKAUF, T. 2002. Vector field metrics based on distance measures of first order critical points. In *Journal of WSCG, Short Communication*, vol. 10, 121–128.

THEISEL, H. 2002. Designing 2D vector fields of arbitrary topology. *Computer Graphics Forum (Eurographics 2002) 21*, 3, 595–604.

TRICOCHE, X., SCHEUERMANN, G., AND HAGEN, H. 2000. A topology simplification method for 2D vector fields. In *Proc. IEEE Visualization 2000*, 359–366.

TRICOCHE, X., SCHEUERMANN, G., AND HAGEN, H. 2001. Continuous topology simplification of planar vector fields. In *Proc. Visualization 01*, 159 – 166.

TRICOCHE, X., SCHEUERMANN, G., AND H.HAGEN. 2001. Topology-based visualization of time-dependent 2D vector fields. In *Data Visualization 2001. Proc. VisSym 01*, 117–126.

TRICOCHE, X., WISCHGOLL, T., SCHEUERMANN, G., AND H.HAGEN. 2002. Topology tracking for the visualization of time-dependent two-dimensional flows. *Computers & Graphics 26*, 249–257.

TROTTS, I., KENWRIGHT, D., AND HAIMES, R. 2000. Critical points at infinity: a missing link in vector field topology. In *Proc. NSF/DoE Lake Tahoe Workshop on Hierarchical Approximation and Geometrical Methods for Scientific Visualization*.

VAN WIJK, J. 1993. Implicit stream surfaces. In *Proc. Visualization 93*, 245–252.

WESTERMANN, R., JOHNSON, C., AND ERTL, T. 2001. Topology-preserving smoothing of vector fields. *IEEE Transactions on Visualization and Computer Graphics 7*, 3, 222–229.

WISCHGOLL, T., AND SCHEUERMANN, G. 2001. Detection and visualization of closed streamlines in planar flows. *IEEE Transactions on Visualization and Computer Graphics 7*, 2, 165–172.

ZHANG, H.-Q., FEY, U., NOACK, B., KÖNIG, M., AND ECKELMANN, H. 1995. On the transition of the cylinder wake. *Phys. Fluids 7*, 4, 779–795.